Human Brain Mapping

Corticostriatal connectivity fingerprints: probability maps based on resting state functional connectivity

Journal:	*Human Brain Mapping*
Manuscript ID	HBM-16-0154.R1
Wiley - Manuscript type:	Research Article
Date Submitted by the Author:	n/a
Complete List of Authors:	Jaspers, Ellen; ETH Zurich, Department of Health Sciences and Technology Balsters, Joshua; ETH Zurich, Department of Health Sciences and Technology Fard Kassraian, Pegah; ETH Zurich, Department of Health Sciences and Technology Mantini, Dante; KU Leuven, Department of Kinesiology Wenderoth, Nicole; ETH Zurich, Department of Health Sciences and Technology; K.U.Leuven, Department of Kinesiology
Keywords:	resting state fMRI, hierarchical clustering, probability maps, corticostriatal connectivity

Corticostriatal connectivity fingerprints: probability maps based on resting state functional connectivity

Jaspers, E.,[1] Balsters, J.H., [1] Kassraian Fard, P., [1] Mantini, D., [1,2] Wenderoth, N. [1,2]

[1] *Neural control of Movement Lab, Department of Health Sciences and Technology, ETH Zurich, Switzerland*

[2] *Movement Control & Neuroplasticity Research Group, Department of Kinesiology, KU Leuven, Belgium*

Institution: ETH Zurich

Switzerland

Corresponding author: Ellen Jaspers

Neural Control of Movement Lab, ETH Zurich

Winterthurerstrasse 190

8057 Zurich, Switzerland

Tel: +41 44 635 61 01

Fax: +41 44 635 61 56

Mail: ellen.jaspers@hest.ethz.ch

Short title: Corticostriatal probability maps

Keywords: resting state fMRI, hierarchical clustering, corticostriatal connectivity, probability maps

Abstract

Over the last decade, structure-function relationships have begun to encompass networks of brain areas rather than individual structures. For example, **corticostriatal** circuits have been associated with sensorimotor, limbic, and cognitive information processing, and damage to these circuits has been shown to produce unique behavioral outcomes in Autism, Parkinson's Disease, Schizophrenia and healthy ageing. However, it remains an open question how abnormal or absent connectivity can be detected at the individual level. Here, we provide a method for clustering gross morphological structures into sub-regions with unique **functional** connectivity fingerprints, and generate network probability maps usable as a baseline to compare individual cases against. We used connectivity metrics derived from resting-state fMRI (N=100), in conjunction with hierarchical clustering methods, to parcellate the striatum into functionally distinct clusters. We identified three highly reproducible striatal sub-regions, across both hemispheres and in an independent replication dataset (N=100) (dice-similarity values 0.40-1.00). Each striatal seed region resulted in a highly reproducible distinct connectivity fingerprint: the putamen showed predominant connectivity with cortical and cerebellar sensorimotor and language processing areas; the ventromedial striatum cluster had a distinct limbic connectivity pattern; the caudate showed predominant connectivity with the thalamus, frontal and occipital areas, and the cerebellum. Our **corticostriatal** probability maps agree with existing connectivity data in humans and non-human primates, and showed a high degree of replication. We believe that these maps offer an efficient tool to further advance hypothesis driven research and provide important guidance when investigating deviant connectivity in neurological patient populations suffering, e.g. stroke or cerebral palsy.

1. Introduction

The anatomy of the human brain has been studied extensively for over a century (Amunts and Zilles, 2006). The first reports of anatomical parcellations used the brains of a few individuals (post-mortem) to identify subdivisions with unique micro-anatomical features (cytoarchitecture) (Brodmann, 1909; Campbell, 1905; Von Economo and Koskinas, 1925). However, because these parcellations were based on only a few individuals, their generalizability remained unclear. Recent technical and methodological advances have enabled scientists to generate anatomical probability maps based on a larger population of individuals (e.g. HarvardOxford (sub-)cortical atlases http://www.cma.mgh.harvard.edu/fsl_atlas.html). These maps highlight that whilst the general anatomical organization is highly reproducible across individuals, there is considerable inter-individual variability regarding the exact boundaries of anatomical subdivisions. A likely reason for this inter-individual variability is that anatomical parcellations, like the HarvardOxford atlases, rely on gross morphological landmarks, and as such they cannot always delineate functional boundaries that represent unique cytoarchitectonic areas (Wig, et al., 2014; Yeo, et al., 2011). There is growing evidence to suggest that understanding the connectivity of a brain region may help to create more accurate parcellations, and generate clearer structure-function relationships that are more informative for brain damage caused by stroke or brain trauma (Amunts, et al., 1999; Burgel, et al., 2006; Hill, et al., 2010).

Growing evidence indicates that complex behavior is rarely mediated by a single brain area in isolation, but rather results from interactions within specialized brain circuits (Otchy, et al., 2015). This has lead to the advent of connectivity-based parcellation, based on the idea that cortical (and subcortical) areas with unique connectivity fingerprints have unique functional roles (Passingham, et al., 2002). In humans, the connectivity fingerprint of a brain region can be determined in-vivo using diffusion imaging methods (Gong, et al., 2009) or resting-state functional MRI (rs-fMRI) (Damoiseaux and Greicius, 2009; Sporns, 2013). Rs-fMRI quantifies spontaneous fluctuations in the blood-oxygenation-level-dependent (BOLD) signal in grey matter regions and enables the detection of large-scale networks of correlated temporal patterns (resting state networks, RSN (Smith, et al., 2012)). Throughout the years, various robust RSNs that exhibit a similar topography have been identified and include areas involved in motor, auditory, and visual or language processing tasks, as well as areas exhibiting “default mode” activity (Biswal, et al., 1995; Damoiseaux, et al., 2006; Greicius, et al., 2003;

Raichle, et al., 2001). Moreover, there is a growing body of evidence showing that rs-fMRI connectivity is significantly changed in a group of patients suffering from brain disorders (Alaerts, et al., 2014; Thiel and Vahdat, 2015). However, it is an open question how abnormal or absent connectivity can be detected at the individual level. Here we aim to provide population maps reflecting **corticostriatal** connectivity patterns, based on rs-fMRI.

We used the striatum as a model structure given that its anatomical connectivity pattern has been extensively described in both non-human primates and in humans (Alexander, et al., 1986; Haber, 2003; Provost, et al., 2015; Robinson, et al., 2012). The striatum consists of the caudate nucleus, the accumbens nucleus and the putamen, which are believed to contribute to cognitive, limbic and sensorimotor activity, respectively. Studies of the putamen suggest that it plays a crucial role in complex motor behaviors, such as implicit motor sequence learning (Doyon, et al., 1996; Grafton, et al., 1995; Jueptner, et al., 1997), and movement initiation (Cunnington, et al., 2002; Jenkins, et al., 2000). The caudate nucleus has stronger anatomical links with the prefrontal cortex, and as such is reported to be involved in more cognitive tasks such as set-shifting processes (Lewis, et al., 2004; Monchi, et al., 2001; Monchi, et al., 2006; Rogers, et al., 2000), rule learning and action-contingency learning (Poldrack, et al., 1999; Seger and Cincotta, 2005), planning of self-initiated actions (Baker, et al., 1996; Owen, et al., 1996; Provost, et al., 2010; van den Heuvel, et al., 2003) and working memory (Lewis, et al., 2004; Monchi, et al., 2006). The nucleus accumbens finally, has been strongly associated with controlling reward and aversive learning (Haber and Knutson, 2010; Hikida, et al., 2016; Monchi, et al., 2001). The whole striatum is affected by various neurological (Albin, et al., 1989; DeLong and Wichmann, 2007; Hoshi, et al., 2005; Wichmann and DeLong, 1996) and psychiatric disorders (Hyman, et al., 2006; Ikemoto, et al., 2015; Simpson, et al., 2010), as well as by healthy aging (Coxon, et al., 2016; Coxon, et al., 2010; Goble, et al., 2011; Goble, et al., 2012), which is accompanied by deviant **corticostriatal** connectivity (Dogan, et al., 2015; Worbe, et al., 2015; Yu, et al., 2013).

Previous research has used independent component analyses to identify connected networks from rs-fMRI data. **This method has the advantage that it is data driven, however, results of different components of the ICA can sometimes be difficult to interpret, especially in case of overlapping components (McKeown et al., 1998) or when an anatomical structure is not part of any component at all (Corbetta, 2012). Moreover, ICA is**

based on the underlying assumption that the maps are spatially independent, which does not necessarily hold for small ROIs. To circumvent this problem, the current study employs two main steps: First, we applied *hierarchical clustering*, a model-free data driven approach, to parcellate the striatum into distinct subregions using the criterion that, first, connectivity fingerprints are similar within each subregion but different between subregions; and, second, that each parcellation is sufficiently reproducible across individuals. Next, we calculated *probability maps of the **corticostriatal** connectivity fingerprint* for each of the striatal subregions.

Here we focused on the striatum, given its crucial involvement in a myriad of diverse processes and brain disorders. However, the presented method is also applicable to other structures and allows the construction of a connectivity fingerprint for the whole-brain while considering inter-individual subject variability typically observed in the healthy population. As such, connectivity probability maps can serve as a reference atlas for deriving anatomical hypotheses regarding brain connectivity, which can subsequently be tested in healthy as well as pathological populations.

2. Methods

2.1 Data

Resting state fMRI (rs-fMRI) data were obtained from the 1000 Functional Connectome Project (http://fcon_1000.projects.nitrc.org/), including only subjects between age 18 and 46 years (N=284). Subjects were further excluded in case of excessive head movements (mean framewise displacement (FD) > 0.5mm) or poor grey matter segmentation, which we quantified based on the squared distance of each image to the sample mean (tool available in the VBM8 toolbox: http://dbm.neuro.uni-jena.de/vbm/download). If this distance was >2SD from the sample mean from the same scanning center, the subject was excluded. After subject exclusion, a total of 2x100 subjects matched for age, gender, and center, were randomly selected for the discovery sample (N=100; 39 male; age 23 $\pm$ 4 years, range 19 to 46 years), and for the replication sample (39 male; age 23 $\pm$ 3 years, range 18 to 43 years).

2.2 Preprocessing

Initial pre-processing was conducted in SPM8 (www.fil.ion.ucl.ac.uk/spm). After co-registering the structural images to the T1 template, data was segmented into grey matter (GM), white matter (WM), and cerebrospinal

fluid (CSF) images using the New Segmentation toolbox (Ashburner, 2007). The DARTEL toolbox was used to create a study specific template, which was warped into MNI space. Functional images were co-registered to the individual structural images, realigned, normalized to MNI space (DARTEL, resliced to 3x3x3mm), and spatially smoothed with a 6mm FWHM smoothing kernel. All analyses were conducted in MNI space, which was further used for generating figures and anatomical localization guided by the anatomy toolbox (Eickhoff, et al., 2005).

Further data pre-processing was conducted using in-house scripts written using MATLAB (MathWorks, Natwick, MA). Data were 'scrubbed' to remove bad data-points (FD >0.5mm or >0.5% differential spatial variance - DVARS) (Power, et al., 2012), and filtered in the band 0.01-0.15Hz, which was considered to contain physiologically relevant information (Balsters, et al., 2013; Baria, et al., 2011). Following Yan et al. (Yan, et al., 2013), head movement was modeled using the Friston 24-parameter approach (Friston, et al., 1996) to remove potential residual head motion signal (6 original regressors generated during realignment, 6 time shifted regressors, and both of these squared) along with the first 3 principle component time series extracted from individual WM and CSF masks (Chai, et al., 2012).

2.3 Data-driven parcellation of the striatum using Hierarchical Clustering

We first applied hierarchical clustering to parcellate the striatum into distinct subregions with unique connectivity fingerprints. Therefore, we created a mask of the left and right striatum separately using masks of the caudate nucleus, putamen, and accumbens nucleus thresholded at 25% probability (Harvard-Oxford Subcortical atlas). For each rs-fMRI dataset, the time-courses of the voxels belonging to the striatal mask and those belonging to all GM voxels in the brain (including the original striatal mask) were separated. Next, the cross-correlation matrix between these two sets of time-courses was calculated, and transformed to z-values using the Fisher's r-to-z transformation (Fisher, 1915; Jenkins, 1968). Each column of this cross-correlation matrix reflects the connectivity of a single striatal voxel with all GM voxels in the brain. The cross-correlation matrices were averaged over all subjects and the resulting matrix was back-transformed to correlation values using the inverse Fisher's transformation, and used as input to a hierarchical clustering algorithm based on an average linkage algorithm. The resulting dendrogram was cut at different levels, representing different numbers of identified clusters. The selection of the optimal number of clusters was based on a combination of

the silhouette measure (Rousseeuw, 1987), and cluster reproducibility for a given solution at the individual subject level. The silhouette value assesses cluster separation by measuring how similar a voxel is to other voxels in the same cluster, compared to voxels in the nearest cluster – thus maximizing within cluster similarity and between cluster differences. A silhouette value was generated for each cut-level of the dendrogram for each individual subject and a t-test was used to determine which cut-levels resulted in the highest silhouette values (cut-levels most representative across individuals). We derived a plot showing the silhouette t-scores for each dendrogram cut-level, and isolated local maxima as potential optimal solutions for the hierarchical clustering. The voxels belonging to a given cluster were then mapped back to brain space. Next, we generated single-subject clustering solutions by running the same hierarchical clustering procedure on individual correlation matrices, and cutting the dendrogram at a position equaling the number of clusters provided by the previous group-level estimates. Finally, we used a procedure described in (Mantini, et al., 2013) to assess the spatial correspondence between clusters derived at the group-level and those derived from individual subjects. We used the Dice similarity measure (Dice, 1945) to assess the correspondence between cluster subregions derived at the group level and those derived from individual subjects. The dice similarity measures the spatial overlap between two segmentations (A,B), with values ranges from 0 (no spatial overlap) to 1 (perfect spatial overlap), and is defined as $Dice(A,B) = 2(A \cap B)/(A+B)$ where $\cap$ is the intersection between both clusters. If a cluster at the individual level matched a cluster at the group mean level it was marked as 1, otherwise it was marked as 0. When a group level cluster was not found at the individual level it was mostly because the cluster was subsumed by an adjacent cluster. Probability maps for each cluster were created by binarizing and summing clusters from each individual subject. Group-level cluster solutions that still showed voxels at 50% probability (i.e. the voxels representing that cluster were present in over 50% of subjects) were retained for further seeding analysis **(striatal clustering probability maps are available for download at http://doi.org/10.5905/ethz-1007-67).**

The hierarchical clustering algorithm was performed for the left and right striatum separately in the discovery and the replication sample, and group-level clustering results were spatially compared with the dice similarity measure (Dice, 1945).

2.4 Comparison of Corticostriatal Functional Connectivity: data driven versus anatomical striatal parcellations

Next we compared connectivity fingerprints derived from a data driven parcellation based on hierarchical clustering and from an anatomical parcellation of the striatum. We used unique striatal seeds of the right striatum, extracted from the 50% probability maps generated through hierarchical clustering, to establish corticostriatal connectivity fingerprints. Results were then compared to corticostriatal connectivity patterns based on right anatomical seeds obtained from the Harvard-Oxford Subcortical atlas (caudate nucleus, putamen, and accumbens nucleus thresholded at 25% probability). For each seed region, a time-course was first extracted (averaged across voxels within the seed) and this time-course was correlated with all GM voxels in the right hemisphere. Scanning center was included as a covariate of no interest at the group level. Group-level connectivity results were voxel-wise FDR uncorrected at $p<0.05$.

2.5 Building population based corticostriatal probability maps

Finally, we aimed to build corticostriatal probability maps at the population level (a flowchart of the procedure is presented in Fig. 1). Individual subject corticostriatal connectivity maps were binarized using a cut-off criterion based on the individual subjects' interhemispheric connectivity. Interhemispheric connectivity was considered to represent 'true' functional connectivity between brain areas (Salvador, et al., 2005) and was calculated as follows for every subject: (1) realigned functional images were normalized to a lower spatial resolution (DARTEL, resliced to 8x8x8mm), and spatially smoothed with a 8mm FWHM smoothing kernel; (2) correlations between time-courses of pairs of symmetrical GM voxels along the anterior-posterior axis were calculated **for all GM voxels (whole-brain)**; (3) the resulting cross-correlation matrices between pairs of symmetrical GM voxels were transformed to z-values using the Fisher's r-to-z transformation (Fisher, 1915; Jenkins, 1968); (4) symmetrical GM voxels were binned according to their distance (10mm bins), and an average z-score was calculated for every entry; (5) **given the dependency of functional connectivity on anatomical distance (Honey, et al., 2009; Salvador, et al., 2005), we only considered z-scores between pairs of GM voxels at least 40mm apart and calculated individual subject thresholds as $z_{thresh} = \mu - 1.5\sigma$ (μ, mean; σ, standard deviation). This z_{thresh}-value, based on interhemispheric connectivity values across the whole hemisphere,** was then used as the cut-off criterion for the individual subjects' connectivity z-maps for every

functional striatal seed. In a final step, binarized maps were re-combined and represented the population based corticostriatal probability maps (available for download at http://doi.org/10.5905/ethz-1007-67).

3. Results

3.1 Data-driven striatal parcellation

Based on the silhouette values of the hierarchical clustering, the right striatum of the discovery sample was parcellated into three, four or fifteen functionally distinct sub-regions (Silhouette values for each cluster solution are presented in Suppl. 1). The three-cluster solution (Fig. 2A) split the striatum into the known anatomical subdivision, i.e. the putamen (cluster 1), the ventromedial striatum (cluster 2) and the caudate nucleus (cluster 3). The four-cluster solution (Fig. 2B) further split the caudate tail (cluster 4) from the caudate body (cluster 3). For the fifteen-cluster solution (Fig. 2C), the putamen was split into an anterior and posterior cluster, containing three and two sub-clusters respectively; the ventromedial striatum was further split into five clusters; the caudate body into four sub-regions, and the caudate tail formed the last cluster. These cluster solutions only represent an average parcellation at the group level. To estimate how well a sub-region is represented across all subjects, we next calculated probability maps of the different cluster solutions. In the four-cluster solution, no unique voxels were left in the caudate tail at 50% probability thresholding; the three remaining seeds were highly similar to those of the three-cluster solution, thresholded at 50%, as shown in the Suppl. material (Suppl. 2: dice similarity values were 0.69, 0.96 and 0.98 for the caudate, ventromedial striatum and putamen cluster, respectively). **For the 15-cluster solution (Fig. 3A), we additionally computed the spatial correlation between the connectivity fingerprints of each of the striatal clusters (Fig. 3B). First, we correlated the time-series of each voxel in the striatum with every grey matter voxel. Next, we calculated the spatial correlation between each of the striatal voxel fingerprints and averaged the correlation over voxels belonging to the same striatal cluster. Spatial correlations were generally high for adjacent clusters, particularly when clusters fell into the same anatomical subdivision (i.e. within the putamen, ventromedial striatum and caudate). In contrast, spatial correlations were low between clusters belonging to different striatal subdivisions.** The three-cluster solution in the discovery sample was highly reproducible, and showed no overlapping voxels at 50% probability thresholding. The probability maps for each of the clusters across the subjects (discovery sample) are presented in **Fig. 4**. The putamen cluster had

highest probability across subjects, ranging up to 98%, followed by the ventromedial striatum cluster (up to 79%) and the caudate cluster (up to 65%).

To further verify the reproducibility of our three-solution clustering results, we next applied the hierarchical cluster analysis to the right striatum of the replication sample (**Fig. 5B**), as well as to the left striatum of the discovery and replication sample (**Fig. 5C and 5D**). Similar to the discovery sample analysis, the right striatum of the replication sample was split into a putamen cluster, a ventromedial striatum cluster and a caudate cluster for the three-cluster solution (dice similarity values for the spatial comparison between the discovery and replication sample were 1.0, 0.41, and 0.63 for the putamen, ventromedial striatum and caudate cluster, respectively). The three-cluster solution for the left striatum also resulted in a putamen, a ventromedial striatum, and a caudate cluster. Spatial comparison between the discovery and the replication sample for the left striatal clustering showed dice similarity values of 0.98, 0.67 and 0.40 for the putamen, ventromedial striatum and caudate cluster, respectively. **Fig. 5** also shows the spatial correlation between the connectivity fingerprints of each of the three clusters (fourth column, cells in the matrix are an average of correlation values for voxels in each cluster). This analysis shows high intra-cluster spatial correlations (diagonal), moderate spatial correlation between connectivity fingerprints of neighboring clusters and low spatial correlations with connectivity fingerprints obtained from other non-adjacent clusters.

3.2 Corticostriatal Functional Connectivity: data driven versus anatomical striatal parcellations

In this analysis, we compared the functional connectivity fingerprint based on anatomical vs. functional seeds to assess the impact of seed selection, as well was the added value of using data-driven striatal parcellations. The anatomical seeds of the striatum were based on the Harvard Oxford Subcortical atlas (**Fig. 6A**); the functional seeds were based on the 50% probability map of the three-solution clustering of the right striatum (**Fig. 6B**). Whilst using a 50% probability threshold reduced the size of the seeds, it also minimized contamination across seeds, which has been shown crucial to attain reliable results in functional connectivity analyses (Smith, et al., 2011). Importantly, the data driven approach revealed a larger cluster for the ventromedial striatum compared to the anatomical parcellation, which is in line with tracing studies in primates (Haber and Knutson, 2010).

3.3 Probability maps of the Corticostriatal Functional Connectivity fingerprint based on interhemispheric connectivity thresholding

In this analysis, we calculated probability maps reflecting **corticostriatal** connectivity fingerprints for each of the three functional clusters (**Fig. 6B** - right striatum, discovery sample). One general problem is how connectivity maps can be binarized, i.e. how to define a cut-off defining which areas are connected and which are not. Here we calculated a cut-off criterion for each subject based on the individual connectivity strength between the hemispheres, which are densely connected via the corpus callosum causing strong symmetric rs-fMRI connectivity patterns. To do so, we calculated the z-transformed correlation values between two symmetric GM voxels of the left and right hemisphere, and considered long-distance connectivity values (> 40mm apart, **Suppl. 3**). The individual cut-off criterion was then determined as $z_{thresh} = \mu - 1.5\sigma$ (μ, mean; σ, standard deviation). For the discovery sample, we found a mean interhemispheric connectivity of μ=1.91 (σ=0.08).

Next we binarized the connectivity map for every subject and each striatal seed region using the individual subject cut-off connectivity values as described above, and calculated the probability map (**Fig. 7**, discovery sample; connectivity map for probability ≥50% is presented). Each striatal seed region resulted in a distinct connectivity fingerprint (**Fig. 7, corticostriatal connectivity probability maps available for download at http://doi.org/10.5905/ethz-1007-67**). The putamen (**Fig. 7A**) shows predominant premotor connectivity (supplementary motor area, middle cingulate cortex, premotor cortex), as well as primary and secondary sensorimotor connectivity (primary motor cortex, primary sensory cortex, insular cortex, operculum) and language processing (supramarginal gyrus). We also found a sensorimotor cerebellar connectivity pattern for the putamen (Lobule VII, VIII, IX; and Lobule VIIb, respectively); the ventromedial striatum cluster (**Fig. 7B**) has a distinct limbic connectivity pattern (amygdala, hippocampus, anterior cingulate cortex); the caudate (**Fig. 7C**) shows predominant connectivity with the thalamus, the frontal pole, the inferior and superior frontal gyrus, the occipital cortex (V1) and the cerebellum (Lobule V, VI, and VIIa crus I). See Suppl. materials for the exact anatomical localization of connectivity pattern (Suppl. Table 4). Results for the replication sample were highly similar and can be found in Suppl. material (**Suppl. 5**).

The direct comparison of the connectivity maps obtained from the anatomical and the functional seeds (using the 60% thresholded probability maps of every seed) showed 94%, 58% and 38% overlapping voxels for the putamen, accumbens/ventromedial striatum and the caudate seed, respectively. However, functional seeds provide a higher degree of unique voxels for each connectivity fingerprint, while the anatomical seeds result in higher overlap (25% overlapping voxels) (Suppl. 6).

4. Discussion

We aimed to determine population maps reflecting **corticostriatal** connectivity patterns based on rs-fMRI **(probability maps of the striatal clustering and the corticostriatal connectivity fingerprint are available for download at http://doi.org/10.5905/ethz-1007-67)**. We first applied hierarchical clustering to the striatum so that voxels with the most similar connectivity fingerprints are assigned to one cluster. However, one challenge inherent to this method is to define a reliable cut-off criterion to determine when the optimal number of clusters has been reached (Eickhoff, et al., 2015). Here, we used a two-step procedure by first finding cluster solutions with a high silhouette value indicating that the connectivity pattern of each given voxel is more similar to other voxels within the same cluster than to voxels in the adjacent clusters. In a second step we tested whether solutions containing relatively large number of clusters would still be reproducible across individuals as well as specifically distinct, i.e. the connectivity fingerprints of different clusters should be non-overlapping. For other criteria to determine the optimal cluster solution see (Eickhoff, et al., 2015). Using this model-free, data driven approach, we identified three functional sub-regions that corresponded to known anatomical subdivisions of the striatum. **Moreover, the sub-regions were highly reproducible across hemispheres (right vs. left clustering, Fig. 5), and across different datasets (discovery vs. replication sample, Fig. 5) and resulted in distinct and highly specific connectivity fingerprints (Fig. 7, and Suppl. 5).**

One advantage of using a clustering approach is that this method provides a cluster solution for each individual, which we subsequently used to calculate probability maps that were thresholded at 50% to create representative, non-overlapping striatal seeds for further analyses (Fig. 4 and 6B). We thereby reduced the risk of inaccurate seed selection and contamination between clusters, and maximized the detection of functional connections (Smith, et al., 2011). Distinct probability maps of the connectivity fingerprint were constructed for every seed (Fig. 7, and Suppl. 5), taking the average individual subject's

interhemispheric connectivity as a cut-off criterion. These probability maps take the inter-individual subject variability into account and, as opposed to standard t- or z-maps, the borders of the connectivity fingerprint are no longer rigid. Averaged interhemispheric z-values ranged from 1.70 to 2.12, similar to previously reported interhemispheric correlations in low and high-resolution data (Honey, et al., 2009).

Previous resting-state studies using comparable approaches for connectivity-based parcellations of the striatum, or a seeding approach with cortical ROIs generated using connectivity-based parcellations, typically reported a more fine-grained group-averaged striatal parcellation (Choi, et al., 2012; Jung, et al., 2014), with the reported number of functionally distinct clusters being much higher than in our study (ranging from two to nine for the caudate, and between three and six for the putamen (Choi, et al., 2012; Jung, et al., 2014). **Thus far, only Jansen et al. took into account inter-individual subject variability and parcellated the striatum using a Bayesian model-based functional clustering approach (Janssen, et al., 2015). These authors identified two caudate clusters, three putamen clusters and the ventromedial striatum, all highly replicable at the single-subject level (Suppl. 7A). However, further exploration of the time-courses of each of these clusters in our discovery sample showed significant mean correlations between time-courses obtained from seeds within the same striatal subdivision (i.e. putamen), whereas seeds belonging to different subdivisions did not show any correlation between their time-courses (Suppl. 7B). The idea that resting functional connectivity differs between the caudate, putamen and nucleus accumbens, but not between clusters within each of this structures is further supported by the time-course correlation matrix based on the 7-cluster parcellation as proposed by Tziortzi et al. (2014) (Suppl. 8A). The mean correlation matrix (z-transformed, discovery sample, p< 0.001) showed highly similar time-courses between clusters within the same striatal subdivisions, whereas time-courses of clusters belonging to different striatal subdivisions did not correlate (Suppl. 8B).**

We identified distinct **corticostriatal** networks for each of the three functional seeds, with highly reproducible probability maps as shown for the discovery and the replication sample (**Fig. 7, Suppl. 5**). We found that the putamen connects preferentially to (pre)motor and sensory cortical areas, and posterior lobules of the cerebellum that have been shown to be connect to sensorimotor areas (Balsters, et al., 2014). The ventromedial striatum connects to parts of the limbic system including hippocampus, amygdala, and anterior

cingulate cortex. The caudate nucleus connects to (pre)frontal areas, the occipital cortex and pre-frontal projecting cerebellar lobules Crus I and Crus II (Balsters, et al., 2014; O'Reilly, et al., 2010).

Our results are consistent with existing anatomical models of **corticostriatal** connectivity, based on anatomical labeling and tracing studies in non-human primates (Alexander, et al., 1986; Nakano, et al., 2000; Parent and Hazrati, 1995; Saint-Cyr, 2003; Selemon and Goldman-Rakic, 1985), as illustrated in Fig. 8. We found predominant connectivity between the putamen and the sensorimotor areas, including the premotor cortex, primary and secondary motor areas and primary and secondary sensory cortex (operculum). **The ventral striatum showed a clear ACC/limbic connectivity pattern as well as some motor connectivity, i.e. the ventral striatum was connected with the ACC, prefrontal and orbitofrontal cortex, limbic structures such as the hippocampus and the amygdala, and motor structures such as (pre)SMA and lateral M1.** Lastly, we also we confirmed the connectivity between the caudate and the (pre)frontal cortex and additionally reported a clear connectivity pattern between putamen, caudate and the cerebellum.

In humans, projections between the striatum and the cortex have been explored using DTI (Draganski, et al., 2008; Leh, et al., 2007; Lehericy, et al., 2004; Tziortzi, et al., 2014; Verstynen, et al., 2012), meta-analyses of cortico-striatal co-activation (Cauda, et al., 2011; Postuma and Dagher, 2006; Robinson, et al., 2012), and rs-fMRI (Choi, et al., 2012; Di Martino, et al., 2008; Janssen, et al., 2015; Jung, et al., 2014). Tractography studies provided evidence of segregated and integrative corticostriatal circuits (Draganski, et al., 2008; Leh, et al., 2007; Lehericy, et al., 2004; Tziortzi, et al., 2014), comparable to the corticostriatal connectivity in non-human primates (Alexander, et al., 1986; Nakano, et al., 2000; Parent and Hazrati, 1995; Saint-Cyr, 2003; Selemon and Goldman-Rakic, 1985). Our results are largely in line with these human tractography findings, as well as previous resting-state studies (Choi, et al., 2012; Di Martino, et al., 2008; Janssen, et al., 2015; Jung, et al., 2014) or meta-analyses of corticostriatal co-activation (Cauda, et al., 2011; Postuma and Dagher, 2006; Robinson, et al., 2012). **However, given that the ventromedial striatum cluster encompasses part of the caudate head, this also resulted in prefrontal and motor connectivity. The ventral striatum has indeed been put forward as a neural interface between the limbic and the motor system (Masahiro, et al., 2015).** Additionally, we identified a visual network connectivity pattern for the caudate cluster, which concurs with non-human primate studies, but thus far has not yet been confirmed in humans based on rs-fMRI (Choi, et al.,

2012; Robinson, et al., 2012). **At lower probability thresholds, the caudate also showed a posterior parietal connectivity fingerprint, whereas the putamen showed most connectivity with the sensorimotor parietal regions (see also Suppl. 9), which is in agreement with previous research (Choi, et al., 2012; Jarbo and Verstynen, 2015).** Lastly, we also demonstrated connectivity with the cerebellum and various subcortical structures in the striatal-cortico-striatal loop, e.g. thalamus, amygdala, hippocampus. Strong connectivity between the amygdala and especially the ventromedial striatum has been reported in both non-human primates (Fudge, et al., 2004; Fudge, et al., 2002; Russchen, et al., 1985) and in humans (Roy, et al., 2009); connectivity between the cerebellum and the striatum, either via the thalamus or directly, has been verified with diffusion imaging (Hoshi, et al., 2005; Leh, et al., 2007). **Taken together, our results show a rostral-to-caudal organization of corticostriatal projections, (Draganski et al., 2008; Badre and Frank, 2012; Verstynen et al., 2012; Verstynen, 2014; Jarbo and Verstynen, 2015). The ventromedial cluster (rostral striatum) mostly projects to rostral areas such as the ACC and the prefrontal and orbitofrontal cortex, whereas the putamen and the caudate cluster (caudal striatum) project more caudally, i.e. sensorimotor areas, frontal and occipital cortex, and the cerebellum (Fig. 7, midline areas).**

Several potential limitations need to be considered when interpreting current study results. **The age range of participants in the current study was limited to 18 to 46 years, due to the use of the functional connectome database, which somewhat limits the generalizability of the proposed probability maps. However, the current probability maps provide a sound baseline representing healthy adults and can thus serve to evaluate changes caused by healthy aging. Moreover, with this paper we also aimed to present a novel method to generate probability maps in any population of interest, and constructing similar probability maps in the elderly population would be a valuable addition to current literature.** Also, the hierarchical clustering and seeding analyses is limited by the resolution of the underlying resting-state data and applying the proposed approach to high-resolution data could be a next logical step. Our parcellation resulted in three functionally distinct clusters with good inter-subject stability. Higher resolution data might allow more fine-grained parcellations that show equal stability over individual subjects. In particular, it might allow the differentiation in clusters involved in the caudate to distinct motor, visual and associative areas and concurrent identification of distinct connectivity fingerprints. Generally, one has to note that the **corticostriatal** connectivity pattern might change according to a general gradient (Haber, 2003; Haber, et al.,

2000), rather than forming distinct connectivity networks. As such, enforcing a hard segmentation of the striatum, as in the current approach, might be a simplification of the "true" underlying connectivity fingerprint. Our results are based on resting-state data, and allow no assumption of directionality of the identified connectivity patterns. **Moreover, Pauli et al. (2016) recently defined corticostriatal associations based on co-activation in task-related responses, combining results across almost 6000 neuroimaging studies, and showed that task-related functional corticostriatal connectivity only partially overlaps with existing resting state parcellations of the striatum (Pauli, et al., 2016). For instance, whilst the resting state connectivity fingerprint of the anterior vs. the posterior putamen does not seem to differ (see also Fig. 3C of this manuscript), these authors showed that both zones do differ functionally: the anterior putamen was more involved in language and other social functions (e.g. empathy), whereas the posterior putamen was found to be more associated with sensorimotor processes, including the processing of painful stimuli. These results suggest that functional striatal zones can only be dissociated in case of co-activation between the striatum and cortical areas, rather than based on resting state functional connectivity (Pauli, et al., 2016).** Lastly, we did not account for the possible contamination of our results due to signal bleeding. For example, Choi et al. have shown that removing the mean signal of the insula shifted the posterior putamen from the ventral attention (adjacent to the insula) to the motor network. However, our results showed a clear connectivity pattern between the putamen and the sensorimotor network, which is in agreement with non-human primate tract-tracing studies (Alexander, et al., 1986; Nakano, et al., 2000; Parent and Hazrati, 1995; Saint-Cyr, 2003; Selemon and Goldman-Rakic, 1985).

5. Conclusions

Our results demonstrated that functional connectivity patterns based on rs-fMRI could be a reliable feature to parcellate the striatum and subsequently identify probability maps of distinct **corticostriatal** circuits. The derived probability maps were highly reproducible and agree well with existing connectivity data in humans and non-human primates. **We believe that these maps offer an effective tool to further advance hypothesis driven research into brain connectivity. In particular, the maps can serve as an independent ROI for any studies investigating corticostriatal circuits in healthy or diseased populations, and thereby avoid the statistical phenomenon of 'double-dipping' (Poldrack and Mumford, 2009).** More importantly, probability

maps might provide important guidance when investigating deviant connectivity in patient populations suffering, for example, from stroke or cerebral palsy (Jaspers, et al., 2015).

Acknowledgements

Funding: E. Jaspers received a Marie Curie Intra European Fellowship within the 7th European Community Framework Programme [FP7-PEOPLE-2013-IEF / Proposal No. 623396]. The authors have no conflict of interest to declare.

References

Alaerts, K., Woolley, D.G., Steyaert, J., Di Martino, A., Swinnen, S.P., Wenderoth, N. (2014) Underconnectivity of the superior temporal sulcus predicts emotion recognition deficits in autism. Soc Cogn Affect Neurosci, 9:1589-600.

Albin, R.L., Young, A.B., Penney, J.B. (1989) The functional anatomy of basal ganglia disorders. Trends in neurosciences, 12:366-75.

Alexander, G.E., DeLong, M.R., Strick, P.L. (1986) Parallel organization of functionally segregated circuits linking basal ganglia and cortex. Annu Rev Neurosci, 9:357-81.

Amunts, K., Schleicher, A., Burgel, U., Mohlberg, H., Uylings, H.B., Zilles, K. (1999) Broca's region revisited: cytoarchitecture and intersubject variability. The Journal of comparative neurology, 412:319-41.

Amunts, K., Zilles, K. (2006) Neuroanatomical Tract Tracing 3: Molecules, Neurons, and Systems. In: Zaborsky, L., Wouterlood, F.G., Lanciego, J.L., editors. Atlases of the human brain: Tools for functional neuroimaging. . New York: Springer. p 556-603.

Baker, S.C., Rogers, R.D., Owen, A.M., Frith, C.D., Dolan, R.J., Frackowiak, R.S., Robbins, T.W. (1996) Neural systems engaged by planning: a PET study of the Tower of London task. Neuropsychologia, 34:515-26.

Balsters, J.H., Laird, A.R., Fox, P.T., Eickhoff, S.B. (2014) Bridging the gap between functional and anatomical features of cortico-cerebellar circuits using meta-analytic connectivity modeling. Hum Brain Mapp, 35:3152-69.

Balsters, J.H., Robertson, I.H., Calhoun, V.D. (2013) BOLD Frequency Power Indexes Working Memory Performance. Front Hum Neurosci, 7:207.

Baria, A.T., Baliki, M.N., Parrish, T., Apkarian, A.V. (2011) Anatomical and functional assemblies of brain BOLD oscillations. The Journal of neuroscience : the official journal of the Society for Neuroscience, 31:7910-9.

Biswal, B., Yetkin, F.Z., Haughton, V.M., Hyde, J.S. (1995) Functional connectivity in the motor cortex of resting human brain using echo-planar MRI. Magn Reson Med, 34:537-41.

Brodmann, K. (1909) Vergleichende Lokalisationslehre der Großhirnrinde : in ihren Prinzipien dargestellt auf Grund des Zellenbaues. Leibzig : Barth.

Burgel, U., Amunts, K., Hoemke, L., Mohlberg, H., Gilsbach, J.M., Zilles, K. (2006) White matter fiber tracts of the human brain: three-dimensional mapping at microscopic resolution, topography and intersubject variability. Neuroimage, 29:1092-105.

Campbell, W.F. (1905) A Laboratory Manual of Human Anatomy. Ann Surg, 42:2.

Cauda, F., Cavanna, A.E., D'Agata, F., Sacco, K., Duca, S., Geminiani, G.C. (2011) Functional connectivity and coactivation of the nucleus accumbens: a combined functional connectivity and structure-based meta-analysis. J Cogn Neurosci, 23:2864-77.

Chai, X.J., Castanon, A.N., Ongur, D., Whitfield-Gabrieli, S. (2012) Anticorrelations in resting state networks without global signal regression. Neuroimage, 59:1420-8.

Choi, E.Y., Yeo, B.T., Buckner, R.L. (2012) The organization of the human striatum estimated by intrinsic functional connectivity. J Neurophysiol, 108:2242-63.

Corbetta, M. (2012) Functional connectivity and neurological recovery. Dev Psychobiol, 54:239-53.

Coxon, J.P., Goble, D.J., Leunissen, I., Van Impe, A., Wenderoth, N., Swinnen, S.P. (2016) Functional Brain Activation Associated with Inhibitory Control Deficits in Older Adults. Cerebral cortex, 26:12-22.

Coxon, J.P., Goble, D.J., Van Impe, A., De Vos, J., Wenderoth, N., Swinnen, S.P. (2010) Reduced basal ganglia function when elderly switch between coordinated movement patterns. Cerebral cortex, 20:2368-79.

Cunnington, R., Windischberger, C., Deecke, L., Moser, E. (2002) The preparation and execution of self-initiated and externally-triggered movement: a study of event-related fMRI. Neuroimage, 15:373-85.

Damoiseaux, J.S., Greicius, M.D. (2009) Greater than the sum of its parts: a review of studies combining structural connectivity and resting-state functional connectivity. Brain structure & function, 213:525-33.

Damoiseaux, J.S., Rombouts, S.A., Barkhof, F., Scheltens, P., Stam, C.J., Smith, S.M., Beckmann, C.F. (2006) Consistent resting-state networks across healthy subjects. Proc Natl Acad Sci U S A, 103:13848-53.

DeLong, M.R., Wichmann, T. (2007) Circuits and circuit disorders of the basal ganglia. Arch Neurol, 64:20-4.

Di Martino, A., Scheres, A., Margulies, D.S., Kelly, A.M., Uddin, L.Q., Shehzad, Z., Biswal, B., Walters, J.R., Castellanos, F.X., Milham, M.P. (2008) Functional connectivity of human striatum: a resting state FMRI study. Cerebral cortex, 18:2735-47.

Dice, L.R. (1945) Measures of the Amount of Ecologic Association Between Species. Ecology, 26:6.

Dogan, I., Eickhoff, C.R., Fox, P.T., Laird, A.R., Schulz, J.B., Eickhoff, S.B., Reetz, K. (2015) Functional connectivity modeling of consistent cortico-striatal degeneration in Huntington's disease. Neuroimage Clin, 7:640-52.

Doyon, J., Owen, A.M., Petrides, M., Sziklas, V., Evans, A.C. (1996) Functional anatomy of visuomotor skill learning in human subjects examined with positron emission tomography. Eur J Neurosci, 8:637-48.

Draganski, B., Kherif, F., Kloppel, S., Cook, P.A., Alexander, D.C., Parker, G.J., Deichmann, R., Ashburner, J., Frackowiak, R.S. (2008) Evidence for segregated and integrative connectivity patterns in the human Basal Ganglia. The Journal of neuroscience : the official journal of the Society for Neuroscience, 28:7143-52.

Eickhoff, S.B., Stephan, K.E., Mohlberg, H., Grefkes, C., Fink, G.R., Amunts, K., Zilles, K. (2005) A new SPM toolbox for combining probabilistic cytoarchitectonic maps and functional imaging data. Neuroimage, 25:1325-35.

Eickhoff, S.B., Thirion, B., Varoquaux, G., Bzdok, D. (2015) Connectivity-based parcellation: Critique and implications. Hum Brain Mapp, 36:4771-92.

Fisher, R.A. (1915) Frequency Distribution of the Values of the Correlation Coefficient in Samples from an Indefinitely Large Population. Biometrika, 10:15.

Friston, K.J., Williams, S., Howard, R., Frackowiak, R.S., Turner, R. (1996) Movement-related effects in fMRI time-series. Magn Reson Med, 35:346-55.

Fudge, J.L., Breitbart, M.A., McClain, C. (2004) Amygdaloid inputs define a caudal component of the ventral striatum in primates. The Journal of comparative neurology, 476:330-47.

Fudge, J.L., Kunishio, K., Walsh, P., Richard, C., Haber, S.N. (2002) Amygdaloid projections to ventromedial striatal subterritories in the primate. Neuroscience, 110:257-75.

Goble, D.J., Coxon, J.P., Van Impe, A., Geurts, M., Doumas, M., Wenderoth, N., Swinnen, S.P. (2011) Brain activity during ankle proprioceptive stimulation predicts balance performance in young and older adults. The Journal of neuroscience : the official journal of the Society for Neuroscience, 31:16344-52.

Goble, D.J., Coxon, J.P., Van Impe, A., Geurts, M., Van Hecke, W., Sunaert, S., Wenderoth, N., Swinnen, S.P. (2012) The neural basis of central proprioceptive processing in older versus younger adults: an important sensory role for right putamen. Hum Brain Mapp, 33:895-908.

Gong, G., He, Y., Concha, L., Lebel, C., Gross, D.W., Evans, A.C., Beaulieu, C. (2009) Mapping anatomical connectivity patterns of human cerebral cortex using in vivo diffusion tensor imaging tractography. Cerebral cortex, 19:524-36.

Grafton, S.T., Hazeltine, E., Ivry, R. (1995) Functional mapping of sequence learning in normal humans. J Cogn Neurosci, 7:497-510.

Greicius, M.D., Krasnow, B., Reiss, A.L., Menon, V. (2003) Functional connectivity in the resting brain: a network analysis of the default mode hypothesis. Proc Natl Acad Sci U S A, 100:253-8.

Haber, S.N. (2003) The primate basal ganglia: parallel and integrative networks. J Chem Neuroanat, 26:317-30.

Haber, S.N., Fudge, J.L., McFarland, N.R. (2000) Striatonigrostriatal pathways in primates form an ascending spiral from the shell to the dorsolateral striatum. The Journal of neuroscience : the official journal of the Society for Neuroscience, 20:2369-82.

Haber, S.N., Knutson, B. (2010) The reward circuit: linking primate anatomy and human imaging. Neuropsychopharmacology, 35:4-26.

Hikida, T., Morita, M., Macpherson, T. (2016) Neural mechanism of the nucleus accumbens circuit in reward and aversive learning. Neurosci Res.

Hill, J., Dierker, D., Neil, J., Inder, T., Knutsen, A., Harwell, J., Coalson, T., Van Essen, D. (2010) A surface-based analysis of hemispheric asymmetries and folding of cerebral cortex in term-born human infants. The Journal of neuroscience : the official journal of the Society for Neuroscience, 30:2268-76.

Honey, C.J., Sporns, O., Cammoun, L., Gigandet, X., Thiran, J.P., Meuli, R., Hagmann, P. (2009) Predicting human resting-state functional connectivity from structural connectivity. Proc Natl Acad Sci U S A, 106:2035-40.

Hoshi, E., Tremblay, L., Feger, J., Carras, P.L., Strick, P.L. (2005) The cerebellum communicates with the basal ganglia. Nat Neurosci, 8:1491-3.

Hyman, S.E., Malenka, R.C., Nestler, E.J. (2006) Neural mechanisms of addiction: the role of reward-related learning and memory. Annu Rev Neurosci, 29:565-98.

Ikemoto, S., Yang, C., Tan, A. (2015) Basal ganglia circuit loops, dopamine and motivation: A review and enquiry. Behav Brain Res, 290:17-31.

Janssen, R.J., Jylanki, P., Kessels, R.P., van Gerven, M.A. (2015) Probabilistic model-based functional parcellation reveals a robust, fine-grained subdivision of the striatum. Neuroimage, 119:398-405.

Jarbo, K., Verstynen T.D. (2015) Converging Structural and Functional Connectivity of Orbitofrontal, Dorsolateral Prefrontal, and Posterior Parietal Cortex in the Human Striatum. J Neurosci, 35:3865-78.

Jaspers, E., Byblow, W.D., Feys, H., Wenderoth, N. (2015) The Corticospinal Tract: A Biomarker to Categorize Upper Limb Functional Potential in Unilateral Cerebral Palsy. Front Pediatr, 3:112.

Jenkins, G.M.W., D.G. (1968) Spectral analysis and its applications. San Fransisco, California. Holden-Day Inc. .

Jenkins, I.H., Jahanshahi, M., Jueptner, M., Passingham, R.E., Brooks, D.J. (2000) Self-initiated versus externally triggered movements. II. The effect of movement predictability on regional cerebral blood flow. Brain : a journal of neurology, 123 (Pt 6):1216-28.

Jueptner, M., Frith, C.D., Brooks, D.J., Frackowiak, R.S., Passingham, R.E. (1997) Anatomy of motor learning. II. Subcortical structures and learning by trial and error. J Neurophysiol, 77:1325-37.

Jung, W.H., Jang, J.H., Park, J.W., Kim, E., Goo, E.H., Im, O.S., Kwon, J.S. (2014) Unravelling the intrinsic functional organization of the human striatum: a parcellation and connectivity study based on resting-state FMRI. PLoS One, 9:e106768.

Leh, S.E., Ptito, A., Chakravarty, M.M., Strafella, A.P. (2007) Fronto-striatal connections in the human brain: a probabilistic diffusion tractography study. Neurosci Lett, 419:113-8.

Lehericy, S., Ducros, M., Van de Moortele, P.F., Francois, C., Thivard, L., Poupon, C., Swindale, N., Ugurbil, K., Kim, D.S. (2004) Diffusion tensor fiber tracking shows distinct corticostriatal circuits in humans. Annals of neurology, 55:522-9.

Lewis, S.J., Dove, A., Robbins, T.W., Barker, R.A., Owen, A.M. (2004) Striatal contributions to working memory: a functional magnetic resonance imaging study in humans. Eur J Neurosci, 19:755-60.

Mantini, D., Corbetta, M., Romani, G.L., Orban, G.A., Vanduffel, W. (2013) Evolutionarily novel functional networks in the human brain? J Neurosci, 33:3259-75.

Masahiro, S., Kenji, K., Takeharu, K., Nobuhiro, M., Susumu, M., Hirotaka, O., Tadashi, Isa., Yukio, N. (2015) Function of the nucleus accumbens in motor control during recovery after spinal cord injury. Science, 350:98-101.

McKeown, M.J., Sejnowski, T.J. (1998) Independent component analysis of fMRI data: examining the assumptions. Hum Brain Mapp, 5-6:368-72.

Monchi, O., Petrides, M., Petre, V., Worsley, K., Dagher, A. (2001) Wisconsin Card Sorting revisited: distinct neural circuits participating in different stages of the task identified by event-related functional magnetic resonance imaging. J Neurosci, 21:7733-41.

Monchi, O., Petrides, M., Strafella, A.P., Worsley, K.J., Doyon, J. (2006) Functional role of the basal ganglia in the planning and execution of actions. Annals of neurology, 59:257-64.

Nakano, K., Kayahara, T., Tsutsumi, T., Ushiro, H. (2000) Neural circuits and functional organization of the striatum. J Neurol, 247 Suppl 5:V1-15.

O'Reilly, J.X., Beckmann, C.F., Tomassini, V., Ramnani, N., Johansen-Berg, H. (2010) Distinct and overlapping functional zones in the cerebellum defined by resting state functional connectivity. Cerebral cortex, 20:953-65.

Otchy, T.M., Wolff, S.B., Rhee, J.Y., Pehlevan, C., Kawai, R., Kempf, A., Gobes, S.M., Olveczky, B.P. (2015) Acute off-target effects of neural circuit manipulations. Nature, 528:358-63.

Owen, A.M., Doyon, J., Petrides, M., Evans, A.C. (1996) Planning and spatial working memory: a positron emission tomography study in humans. Eur J Neurosci, 8:353-64.

Parent, A., Hazrati, L.N. (1995) Functional anatomy of the basal ganglia. I. The cortico-basal ganglia-thalamo-cortical loop. Brain Res Brain Res Rev, 20:91-127.

Passingham, R.E., Stephan, K.E., Kotter, R. (2002) The anatomical basis of functional localization in the cortex. Nat Rev Neurosci, 3:606-16.

Poldrack, R.A., Mumford, J.A. (2009) Independence in ROI analysis: where is the voodoo? Soc Cogn Affect Neurosci, 4:208-13.

Poldrack, R.A., Prabhakaran, V., Seger, C.A., Gabrieli, J.D. (1999) Striatal activation during acquisition of a cognitive skill. Neuropsychology, 13:564-74.

Postuma, R.B., Dagher, A. (2006) Basal ganglia functional connectivity based on a meta-analysis of 126 positron emission tomography and functional magnetic resonance imaging publications. Cerebral cortex, 16:1508-21.

Power, J.D., Barnes, K.A., Snyder, A.Z., Schlaggar, B.L., Petersen, S.E. (2012) Spurious but systematic correlations in functional connectivity MRI networks arise from subject motion. Neuroimage, 59:2142-54.

Provost, J.S., Hanganu, A., Monchi, O. (2015) Neuroimaging studies of the striatum in cognition Part I: healthy individuals. Front Syst Neurosci, 9:140.

Provost, J.S., Petrides, M., Monchi, O. (2010) Dissociating the role of the caudate nucleus and dorsolateral prefrontal cortex in the monitoring of events within human working memory. Eur J Neurosci, 32:873-80.

Raichle, M.E., MacLeod, A.M., Snyder, A.Z., Powers, W.J., Gusnard, D.A., Shulman, G.L. (2001) A default mode of brain function. Proc Natl Acad Sci U S A, 98:676-82.

Robinson, J.L., Laird, A.R., Glahn, D.C., Blangero, J., Sanghera, M.K., Pessoa, L., Fox, P.M., Uecker, A., Friehs, G., Young, K.A., Griffin, J.L., Lovallo, W.R., Fox, P.T. (2012) The functional connectivity of the human caudate: an application of meta-analytic connectivity modeling with behavioral filtering. Neuroimage, 60:117-29.

Rogers, R.D., Andrews, T.C., Grasby, P.M., Brooks, D.J., Robbins, T.W. (2000) Contrasting cortical and subcortical activations produced by attentional-set shifting and reversal learning in humans. J Cogn Neurosci, 12:142-62.

Rousseeuw, P.J. (1987) Silhouettes: A graphical aid to the interpretation and validation of cluster analysis. Journal of Computational and Applied Mathematics, 20:13.

Roy, A.K., Shehzad, Z., Margulies, D.S., Kelly, A.M., Uddin, L.Q., Gotimer, K., Biswal, B.B., Castellanos, F.X., Milham, M.P. (2009) Functional connectivity of the human amygdala using resting state fMRI. Neuroimage, 45:614-26.

Russchen, F.T., Bakst, I., Amaral, D.G., Price, J.L. (1985) The amygdalostriatal projections in the monkey. An anterograde tracing study. Brain Res, 329:241-57.

Saint-Cyr, J.A. (2003) Frontal-striatal circuit functions: context, sequence, and consequence. J Int Neuropsychol Soc, 9:103-27.

Salvador, R., Suckling, J., Coleman, M.R., Pickard, J.D., Menon, D., Bullmore, E. (2005) Neurophysiological architecture of functional magnetic resonance images of human brain. Cerebral cortex, 15:1332-42.

Seger, C.A., Cincotta, C.M. (2005) The roles of the caudate nucleus in human classification learning. The Journal of neuroscience : the official journal of the Society for Neuroscience, 25:2941-51.

Selemon, L.D., Goldman-Rakic, P.S. (1985) Longitudinal topography and interdigitation of corticostriatal projections in the rhesus monkey. J Neurosci, 5:776-94.

Simpson, E.H., Kellendonk, C., Kandel, E. (2010) A possible role for the striatum in the pathogenesis of the cognitive symptoms of schizophrenia. Neuron, 65:585-96.

Smith, S.M., Miller, K.L., Moeller, S., Xu, J., Auerbach, E.J., Woolrich, M.W., Beckmann, C.F., Jenkinson, M., Andersson, J., Glasser, M.F., Van Essen, D.C., Feinberg, D.A., Yacoub, E.S., Ugurbil, K. (2012) Temporally-independent functional modes of spontaneous brain activity. Proc Natl Acad Sci U S A, 109:3131-6.

Smith, S.M., Miller, K.L., Salimi-Khorshidi, G., Webster, M., Beckmann, C.F., Nichols, T.E., Ramsey, J.D., Woolrich, M.W. (2011) Network modelling methods for FMRI. Neuroimage, 54:875-91.

Sporns, O. (2013) The human connectome: origins and challenges. Neuroimage, 80:53-61.

Thiel, A., Vahdat, S. (2015) Structural and resting-state brain connectivity of motor networks after stroke. Stroke, 46:296-301.

Tziortzi, A.C., Haber, S.N., Searle, G.E., Tsoumpas, C., Long, C.J., Shotbolt, P., Douaud, G., Jbabdi, S., Behrens, T.E., Rabiner, E.A., Jenkinson, M., Gunn, R.N. (2014) Connectivity-based functional analysis of dopamine release in the striatum using diffusion-weighted MRI and positron emission tomography. Cerebral cortex, 24:1165-77.

van den Heuvel, O.A., Groenewegen, H.J., Barkhof, F., Lazeron, R.H., van Dyck, R., Veltman, D.J. (2003) Frontostriatal system in planning complexity: a parametric functional magnetic resonance version of Tower of London task. Neuroimage, 18:367-74.

Verstynen, T.D., Badre, D., Jarbo, K., Schneider, W. (2012) Microstructural organizational patterns in the human corticostriatal system. J Neurophysiol, 107:2984-95.

Von Economo, C., Koskinas, G.N. (1925) Die cytoarchitektonik der Hirnrinde des erwaschenen Menschen. Berlin. Springer.

Wichmann, T., DeLong, M.R. (1996) Functional and pathophysiological models of the basal ganglia. Current opinion in neurobiology, 6:751-8.

Wig, G.S., Laumann, T.O., Petersen, S.E. (2014) An approach for parcellating human cortical areas using resting-state correlations. Neuroimage, 93 Pt 2:276-91.

Worbe, Y., Marrakchi-Kacem, L., Lecomte, S., Valabregue, R., Poupon, F., Guevara, P., Tucholka, A., Mangin, J.F., Vidailhet, M., Lehericy, S., Hartmann, A., Poupon, C. (2015) Altered structural connectivity of cortico-striato-pallido-thalamic networks in Gilles de la Tourette syndrome. Brain : a journal of neurology, 138:472-82.

Yan, C.G., Cheung, B., Kelly, C., Colcombe, S., Craddock, R.C., Di Martino, A., Li, Q., Zuo, X.N., Castellanos, F.X., Milham, M.P. (2013) A comprehensive assessment of regional variation in the impact of head micromovements on functional connectomics. Neuroimage, 76:183-201.

Yeo, B.T., Krienen, F.M., Sepulcre, J., Sabuncu, M.R., Lashkari, D., Hollinshead, M., Roffman, J.L., Smoller, J.W., Zollei, L., Polimeni, J.R., Fischl, B., Liu, H., Buckner, R.L. (2011) The organization of the human cerebral cortex estimated by intrinsic functional connectivity. J Neurophysiol, 106:1125-65.

Yu, R., Liu, B., Wang, L., Chen, J., Liu, X. (2013) Enhanced functional connectivity between putamen and supplementary motor area in Parkinson's disease patients. PLoS One, 8:e59717.

Figure legends

Figure 1.

Flowchart of the calculation of the probability maps for the connectivity fingerprint, based on interhemispheric connectivity thresholding (figure shows example for the putamen functional cluster, probability map 50%).

Figure 2.

Hierarchical clustering of the right striatum (discovery sample) into functionally distinct sub-regions: (A) 3-cluster solution, splitting the striatum into the putamen (red), ventromedial striatum (green), and the caudate (pink); (B) 4-cluster solution, separating the caudate tail (yellow) from the caudate body (pink), while the ventromedial striatum (green) and the putamen (red) remain; (C) 15-cluster solution, further subdividing the putamen into 5 sub-regions, the ventromedial striatum into 5 sub-regions and the caudate body into 4 sub-regions, while the caudate tail remains 1 cluster.

Figure 3.

Right striatum functional clusters based on hierarchical clustering: (A) 15-cluster solution (discovery sample); (B) Spatial correlation between connectivity fingerprints of each of the 15 clusters (cells in the matrix are an average of correlation values for voxels in each cluster). High spatial correlations were found between adjacent clusters in the putamen, ventromedial striatum and caudate, whilst very low correlations were found between clusters belonging to separate striatal subdivisions (caudate, ventromedial striatum, putamen).

Figure 4.

Probability maps of the three-cluster solution of the right striatum (discovery sample), presented for each of the clusters separately (maps are thresholded at 25%, as indicated in the color bar with |).

Figure 5.

Hierarchical clustering of the striatum into three functionally distinct clusters, i.e. a putamen (red), a ventromedial striatum (green) and a caudate cluster (pink). (A) right striatum, discovery sample; (B) right

striatum, replication sample; (C) left striatum, discovery sample; (D) left striatum, replication sample; The 4th column represents the spatial correlation between connectivity fingerprints of each of the three clusters (cells in the matrix are an average of correlation values for voxels in each cluster). This analysis shows high intra-cluster spatial correlations (diagonal), moderate spatial correlation between connectivity fingerprints of neighboring clusters and low spatial correlations with connectivity fingerprints obtained from other non-adjacent clusters. Labels are as follows: put is the putamen cluster (red), veStr is the ventromedial striatum cluster (green), and caud is the caudate cluster (pink).

Figure 6.

Rendering of striatal seeds. (A) Anatomical parcellation based on the Harvard Oxford subcortical atlas (25% probability) showing the putamen (cyan), accumbens (green) and the caudate (yellow); (B) Functional parcellation taken from the 50% probability map: putamen (red), ventromedial striatum (green), and caudate cluster (pink).

Figure 7.

Corticostriatal connectivity maps at probability >50% (discovery sample, three-cluster striatal seeds). Results show a clear anterior-posterior gradient, with premotor/sensorimotor, limbic/ACC and prefrontal/visual/cerebellar connectivity for the putamen (A), ventromedial striatum (B) and caudate (C), respectively. Black dotted line indicates seed location.

Figure 8.

Schematic overview of primate **corticostriatal** connectivity based on tracer studies in primates (Alexander et al., 1986; Haber and Knutson, 2010) (black arrows) and summary of current study results (dotted arrows).

M1: motor cortex; PM: premotor cortex; SS: somatosensory cortex; SMA: supplementary motor area; vmPFC: ventromedial prefrontal cortex; OFC: orbitofrontal cortex; DPFC: dorsal prefrontal cortex; DLPFC: dorso-lateral prefrontal cortex; LOFC: lateral orbitofrontal cortex; PPC: posterior parietal cortex; APA: arcuate premotor area; ITG: inferior temporal gyrus; STG: superior temporal gyrus; ACC anterior cingulate cortex; LIMBIC: refers to limbic structures, e.g. hippocampus, amygdala.

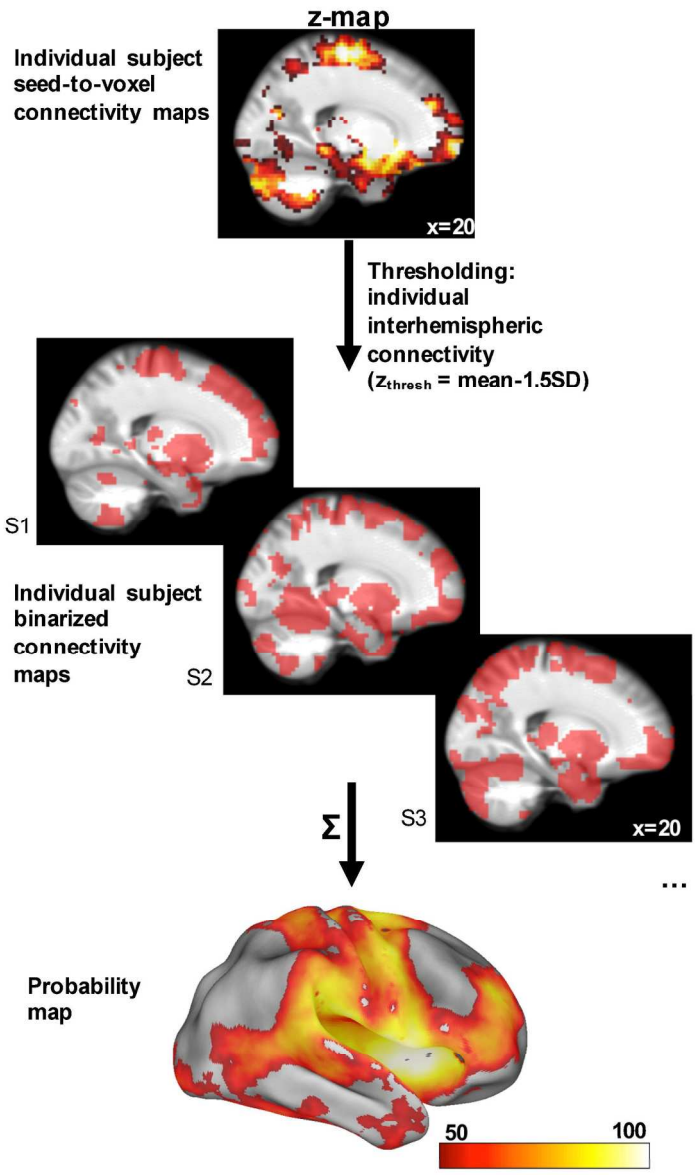

Figure 1.
Flowchart of the calculation of the probability maps for the connectivity fingerprint, based on interhemispheric connectivity thresholding (figure shows example for the putamen functional cluster, probability map 50%).
Fig. 1
149x249mm (300 x 300 DPI)

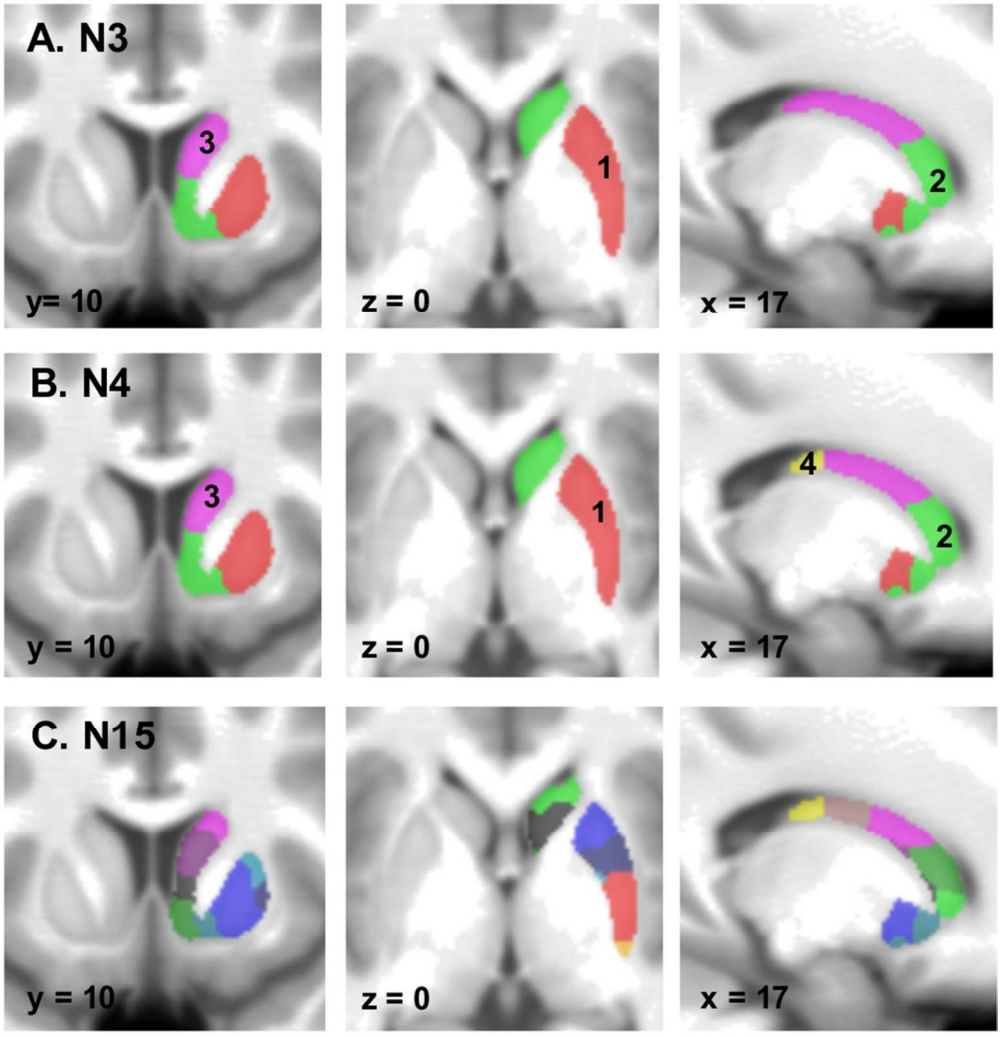

Figure 2.
Hierarchical clustering of the right striatum (discovery sample) into functionally distinct sub-regions: (A) 3-cluster solution, splitting the striatum into the putamen (red), ventromedial striatum (green), and the caudate (pink); (B) 4-cluster solution, separating the caudate tail (yellow) from the caudate body (pink), while the ventromedial striatum (green) and the putamen (red) remain; (C) 15-cluster solution, further subdividing the putamen into 5 sub-regions, the ventromedial striatum into 5 sub-regions and the caudate body into 4 sub-regions, while the caudate tail remains 1 cluster.
Fig. 2
92x96mm (300 x 300 DPI)

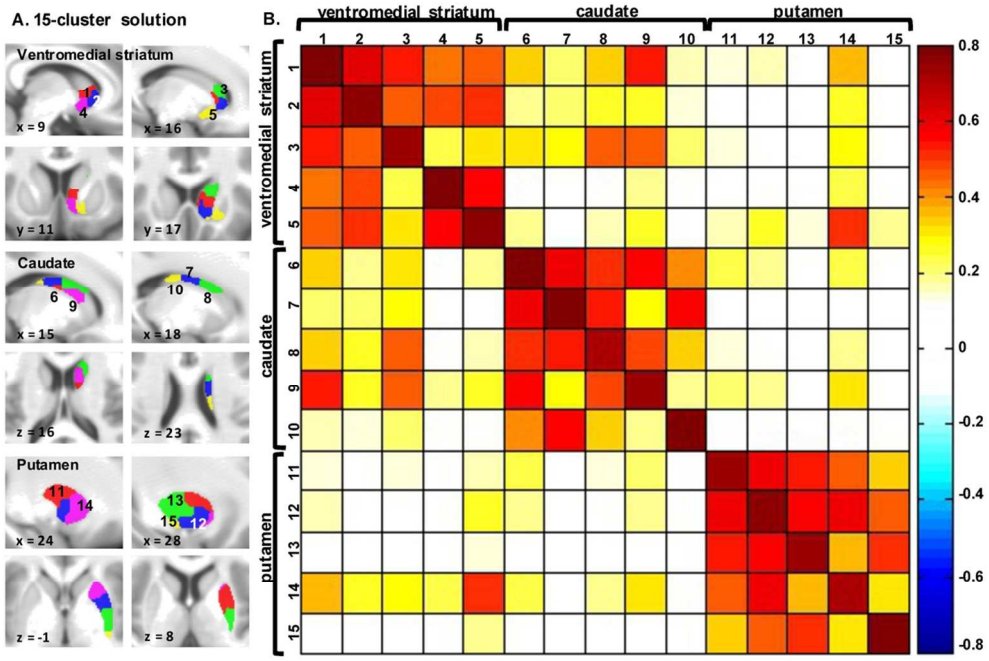

Figure 3.
Right striatum functional clusters based on hierarchical clustering: (A) 15-cluster solution (discovery sample); (B) Spatial correlation between connectivity fingerprints of each of the 15 clusters (cells in the matrix are an average of correlation values for voxels in each cluster). High spatial correlations were found between adjacent clusters in the putamen, ventromedial striatum and caudate, whilst very low correlations were found between clusters belonging to separate striatal subdivisions (caudate, ventromedial striatum, putamen).
Fig. 3A
113x77mm (300 x 300 DPI)

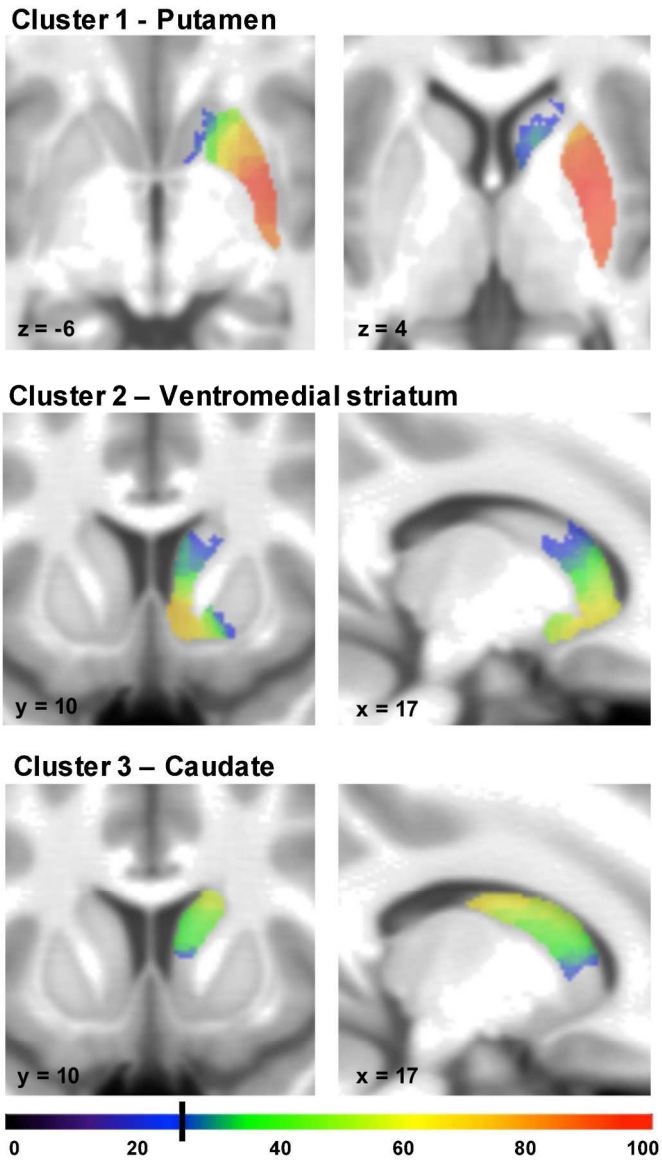

Figure 4.
Probability maps of the three-cluster solution of the right striatum (discovery sample), presented for each of the clusters separately (maps are thresholded at 25%, as indicated in the color bar with |).
Fig. 4
151x262mm (300 x 300 DPI)

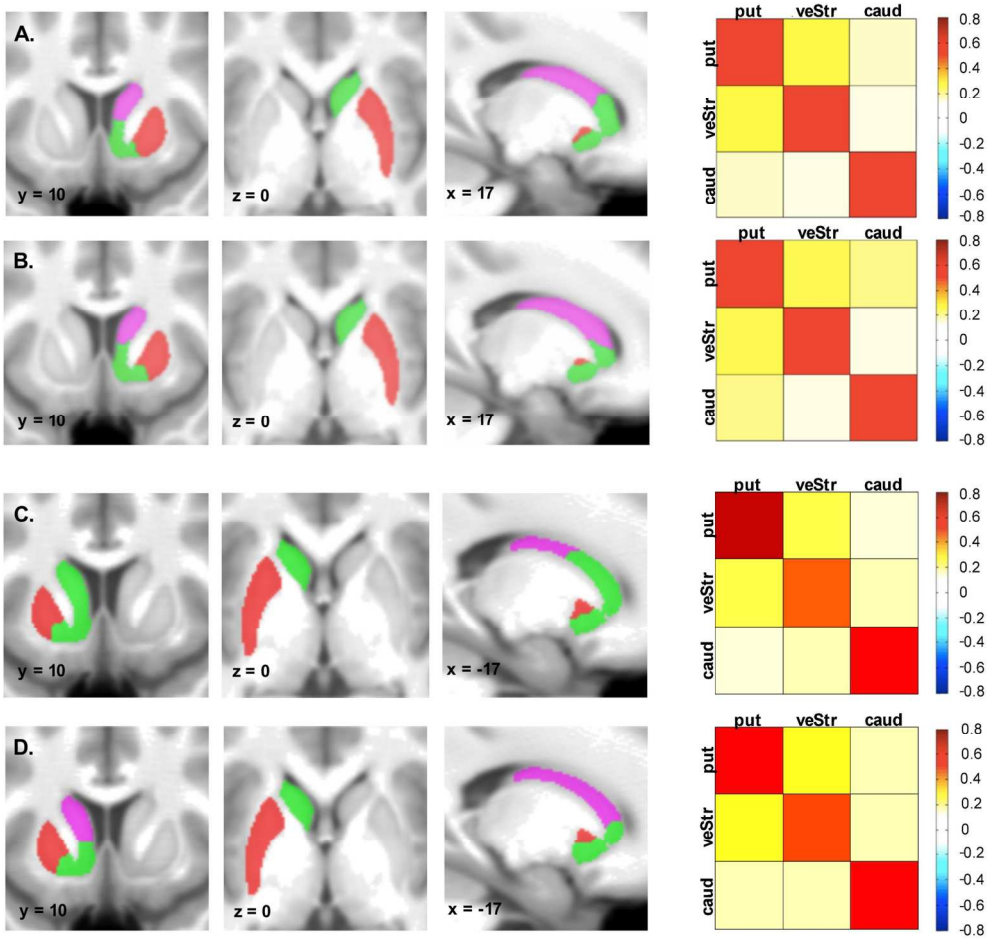

Figure 5.
Hierarchical clustering of the striatum into three functionally distinct clusters, i.e. a putamen (red), a ventromedial striatum (green) and a caudate cluster (pink). (A) right striatum, discovery sample; (B) right striatum, replication sample; (C) left striatum, discovery sample; (D) left striatum, replication sample; The 4th column represents the spatial correlation between connectivity fingerprints of each of the three clusters (cells in the matrix are an average of correlation values for voxels in each cluster). This analysis shows high intra-cluster spatial correlations (diagonal), moderate spatial correlation between connectivity fingerprints of neighboring clusters and low spatial correlations with connectivity fingerprints obtained from other non-adjacent clusters. Labels are as follows: put is the putamen cluster (red), veStr is the ventromedial striatum cluster (green), and caud is the caudate cluster (pink).
Fig. 5
157x149mm (300 x 300 DPI)

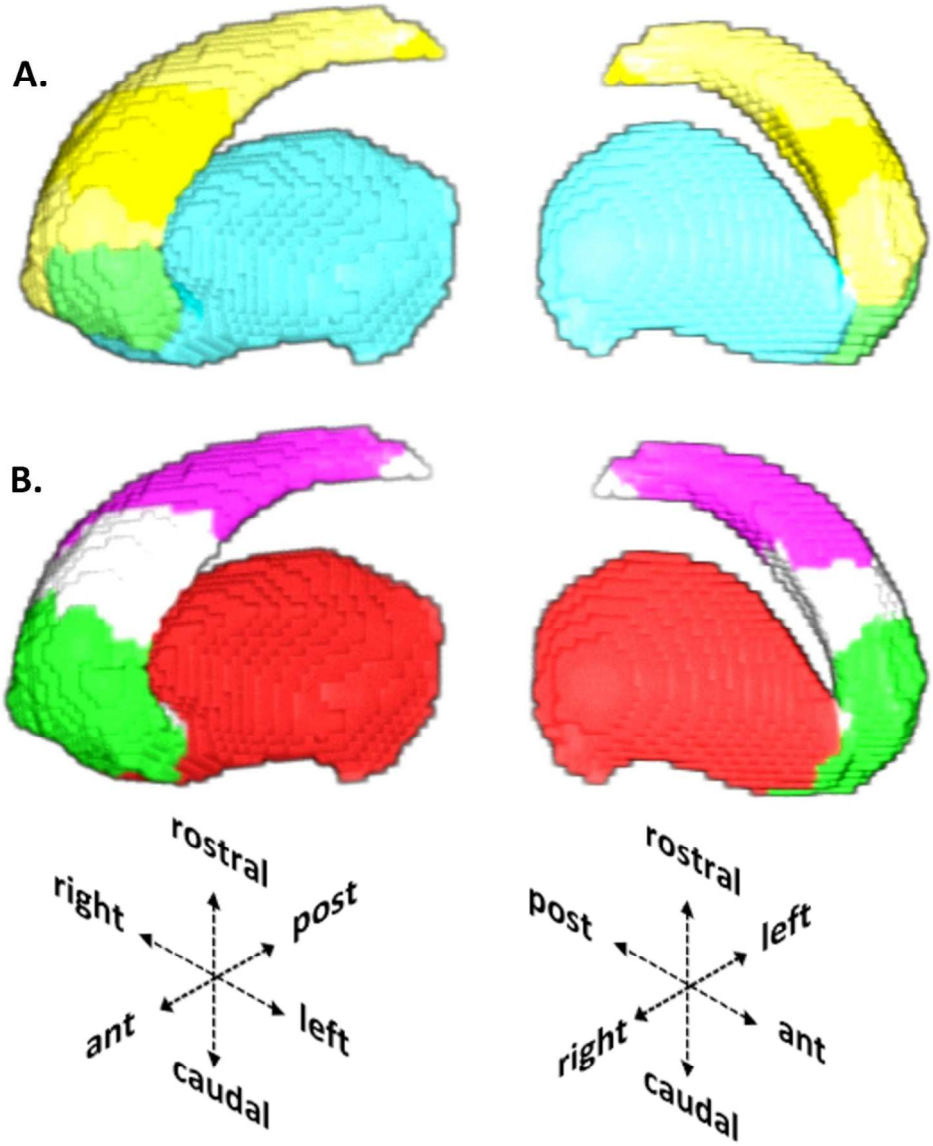

Figure 6.
Rendering of striatal seeds. (A) Anatomical parcellation based on the Harvard Oxford subcortical atlas (25% probability) showing the putamen (cyan), accumbens (green) and the caudate (yellow); (B) Functional parcellation taken from the 50% probability map: putamen (red), ventromedial striatum (green), and caudate cluster (pink).
Fig. 6
103x126mm (300 x 300 DPI)

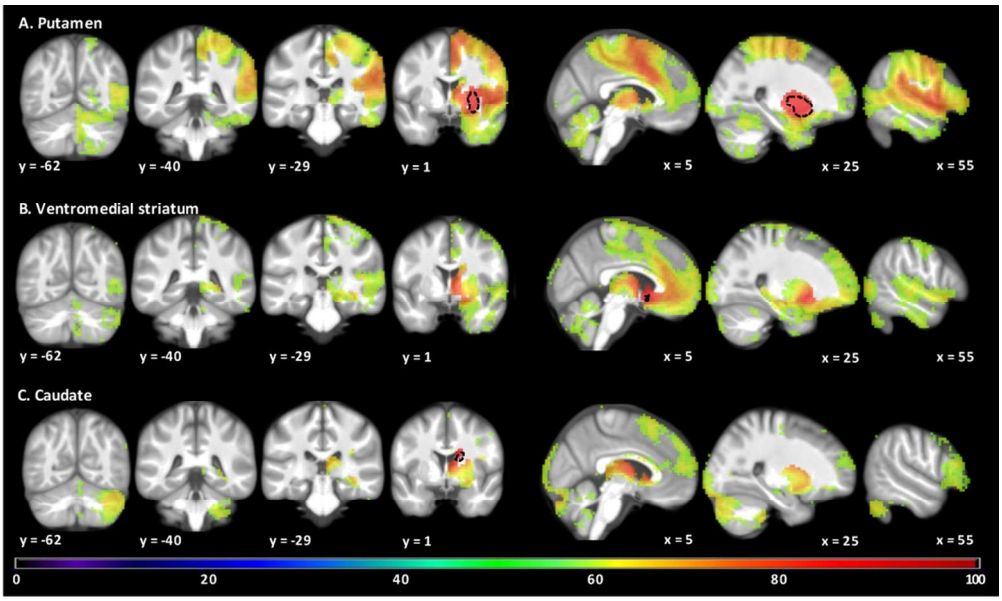

Figure 7.
Corticostriatal connectivity maps at probability >50% (discovery sample, three-cluster striatal seeds). Results show a clear anterior-posterior gradient, with premotor/sensorimotor, limbic/ACC and prefrontal/visual/cerebellar connectivity for the putamen (A), ventromedial striatum (B) and caudate (C), respectively. Black dotted line indicates seed location.
Fig. 7
98x58mm (300 x 300 DPI)

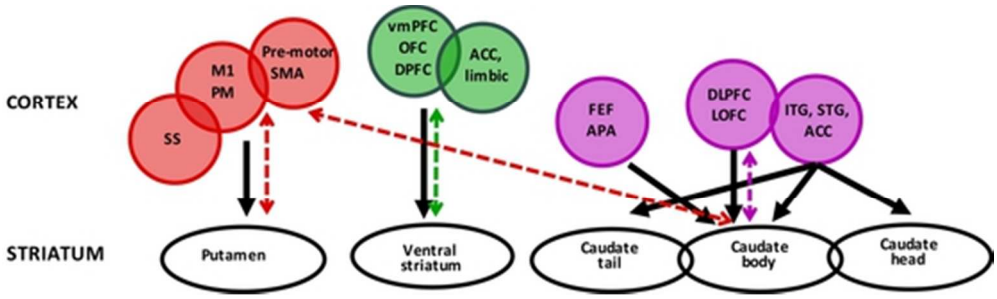

Figure 8.
Schematic overview of primate corticostriatal connectivity based on tracer studies in primates (Alexander et al., 1986; Haber and Knutson, 2010) (black arrows) and summary of current study results (dotted arrows). M1: motor cortex; PM: premotor cortex; SS: somatosensory cortex; SMA: supplementary motor area; vmPFC: ventromedial prefrontal cortex; OFC: orbitofrontal cortex; DPFC: dorsal prefrontal cortex; DLPFC: dorso-lateral prefrontal cortex; LOFC: lateral orbitofrontal cortex; PPC: posterior parietal cortex; APA: arcuate premotor area; ITG: inferior temporal gyrus; STG: superior temporal gyrus; ACC anterior cingulate cortex; LIMBIC: refers to limbic structures, e.g. hippocampus, amygdala.
Fig. 8
47x13mm (300 x 300 DPI)